Article

Not peer-reviewed version

# Numerical investigation on a solar heating system with solar tower receiver and seasonal storage in north China: Dynamic performance assessment and operation strategies analysis

Xiaoxia Li *, Husheng Qiu , Zhifeng Wang *, Jinping Li , Guobin Yuan , Xiao Guo , Longfei Chen

Posted Date: 17 July 2023

doi: 10.20944/preprints202307.1064.v1

Keywords: Solar heating system; Dynamic performance; Seasonal thermal storage; Underground water pit seasonal storage; Operation strategies

*Article*

# Numerical Investigation on a Solar Heating System with Solar Tower Receiver and Seasonal Storage in North China: Dynamic Performance Assessment and Operation Strategies Analysis

**Xiaoxia Li [1,2,3,4,6,*], Husheng Qiu [1,3,4], Zhifeng Wang [1,5,*], Jinping Li [1,2,3], Guobin Yuan [1,2,3], Xiao Guo [1,2,3] and Lifeng Jin [1,3,4]**

[1] School of Energy and Power Engineering, Lanzhou University of Technology, Lanzhou 730050, China
[2] Key Laboratory of Solar Power System Engineering, Gansu, Jiuquan Vocational and Technical College, Jiuquan, 735000, China
[3] Western China Energy and Environment Research Center, Lanzhou University of Technology, Lanzhou 730050, China
[4] China Northwest Collaborative Innovation Center of Low-carbon Unbanization Techonlogies, Lanzhou 730050, China
[5] Key Laboratory of Solar Thermal Energy and Photovoltaic System, Institute of Electrical Engineering, Chinese Academy of Sciences, No. 6 Beiertiao, Zhongguancun, Beijing 100190, China
[6] Urumqi Sikorsk Energy Contract Management Professional Technical Service Co., Ltd., Urumqi Sikorsk 830011, China
* Correspondence: lixx@lut.edu.cn (X.L.); wangzf@mail.iee.ac.cn (Z.W.)

**Abstract:** Solar heating technology is a promising solution to promote China to achieve the "3060 double carbon" target as soon as possible. And seasonal thermal storage (STS) can effectively solve the mismatch problem of solar heating systems between the supply and demand of thermal energy. Due to the instability of solar radiation resources and heat demand, it is necessary to analyze the dynamic response characteristics and operation strategy optimization of the system under different operation stages. Yet, related studies are still scarce. The aim of this paper is to study the switching mechanism of operation modes and the transitive relation of system energy in different operation stages based on a pilot solar heating system with STS in Huangdicheng, north China. And the impact of different heating strategies on system performance was also analyzed with a dynamic simulated method in TRNSYS. Results showed that the solar fraction of the system could reach 89.4% in the third year, which was 3.6% higher than the first year. The quality-quantity heating operation strategies can be effective ways to improve the discharge efficiency of STS and the system performance without heat pump. The electricity consumption of the pump on the heating side could be significantly reduced by 44.6% compared with the quality control. Ultimately, the findings in this paper are valuable for the optimization of the operation of solar heating system.

**Keywords:** solar heating system; dynamic performance; seasonal thermal storage; underground water pit seasonal storage; operation strategies

## 1. Introduction

About 50% of the total final energy consumption in the world attributes to the heat used in the residential and industrial sectors. With the rapid development of urbanization, the heating area of urban buildings in northern China increased from 5 billion $m^2$ to 15.6 billion $m^2$ from 2001 to 2020. In 2020, urban heating energy consumption in northern China was 214 million tons of standard coal, accounting for 20.2% of the total building energy consumption [1]. And heating is not only an energy consumption issue but also a livelihood issue. In northern China, the average outdoor temperature in the heating season is relatively low. For example, the calculated outdoor temperature for heating in Zhangjiakou, Hebei is -13.6°C. In addition, space heating still relies on traditional energy sources such as coal and natural gas in northern China. While the spatial distribution of solar energy

 doi:10.20944/preprints202307.1064.v1



resources in China is highly consistent with traditional centralized heating areas, especially in the northern regions. Therefore, the development of solar heating in northern China not only has demand advantages but also resource advantages.

Solar heating systems with storage is very common. The salt gradient solar pond (SGSP) is one of these systems. Rghif et al. conducted extensive in-depth research to further improve the performance and efficiency of SGSP systems[2–5]. On the other hand, as STS can effectively solve the mismatch between the supply and demand of thermal energy in time and space. And the solar fraction and operational stability of the solar heating systems can be significantly improved. Thus, seasonal thermal storage technology has attracted increasing attention. Many researchers conducted performance analysis and operation strategies analysis.

Reasonable performance analysis of the system is the premise of establishing a solar heating system with STS. Tosatto et al. studied the environmental aspect and technical performance of large-scale thermal energy storage coupled with a heat pump in district heating systems. Results showed that the integration of the heat pump proves to be effective in increasing the thermal storage efficiency by 6% (from 87%) compared to the reference case without a heat pump in the case of an insulated tank thermal storage, and by 16% (from 64%) in case of an insulated shallow pit [6]. Narula et al. present a new simulation method to assess a simulation method for modeling hourly energy flows in a district heating system integrated with STS. Based on the validation with the measured values of Friedrichshafen and Marstal, the annual energy flow could be closely replicated, while large monthly differences between simulations and measurements were reported [7]. Ushamah et al. compared the performance of district heating systems with STS under different climatic conditions and identified the best suitable solar thermal technology. The conclusion was that the zone with a continental semi-arid climate was selected as the most suitable, with a STS efficiency of 61% and a solar fraction of 91% [8]. Kim et al. evaluated the technology and economic performance of a hybrid renewable energy system with STS in South Korea using dynamic simulations and experimental results. Results showed that the proposed system reduced $CO_2$ emission by up to 61% compared with a centralized heat pump system and enhanced primary energy savings by up to 73% compared with gas-fired boilers [9]. Chu et al. assessed the technically and economically feasible of a solar assisted precinct level heating system with STS for Australian cities, the results demonstrated that the proposed system could achieve technical and economic targets in all five Australian cities considered with optimal collector area and storage volume [10]. Renaldi et al. established a validated simulation model to study the yearly performance of a solar district heating system with STS in UK. According to the study, solar collectors and long-term storage size have a more significant influence on the techno-economic metrics than short-term storage [11]. Zhang et al. experimental investigated the dynamic thermal behaviors of a combined solar and ground source heat pump (SGHP) system with a dual storage tank for a single-family house on typical days [12].

The design of reasonable operation strategies is an important factor to realize the stable operation of the system, the efficient integration of all parts of the system, and the reduction of system cost. Maragna et al. introduced a multi-source system and overall control strategies combining solar thermal collectors, borehole thermal energy storage, a heap pump, and a backup boiler. Monthly and typical day system performance were also analyzed, and the results illustrated that the energy balance is sensitive to the choice of the parameter values used for the controls [13]. Li et al. compared the influence of control strategies of the solar collection subsystem on the system performance in the non-heating system. Note that the control strategies were significant for improving the heat collection performance of solar receiver, and also the stratification of STS has an impact on the collection efficiency of the receiver, especially at the end of the non-heating season [14]. Villasmil et al. studied the performance of a solar heating system with STS under the variation of solar collector control strategies. The results showed that the required storage volume was minimized through the application of a low-flow controller, while the use of a high-flow controller or variable-flow controller led to an increase of 42 and 8% in the storage volume, respectively [15]. Wang et al. proposed a feedback control strategy for an integrated solar and air-source heat pump water heating system, where the temperature of the heat storage tank was compared with the set temperature curve to

determine whether to use an air-source heat pump for auxiliary heating. The reliability of the control strategy had been verified through simulation and experimental research, and the operational efficiency of the collector and air source heat pump had been significantly improved [16]. Zhao et al. proposed a system operation control strategy and studied the annual operating performance of a solar heating system with seasonal water pool thermal storage in cold regions of China. Analysis revealed that the solar fraction of the system with the adjustment operation strategy during the heating period can reach 78.5% [17].

As mentioned above, many scholars have done a lot of work concerning the performance assessment of the solar heating system with STS, and most previous studies focused on the techno-economic analysis based on the annual energy balance of the system, or the operation strategies analysis aiming at the solar circuit or thermal storage circuit. However, due to the instability of solar radiation resources and heat demand, it is necessary to balance the heat supply and demand throughout the year, and also to analyze the dynamic response characteristics and heating quality on a minute timescale. Yet, related studies are still scarce.

To fill the gaps mentioned above, based on a pilot solar heating system with STS in Huangdicheng, north China, a dynamic performance evaluation and operation strategies study is presented in this paper. The main novelties of the present study can be clarified as:

(1) The system's dynamical performance was analyzed with a dynamic simulated method in a typical day or typical operation modes, and the switch mechanism between multiple operation modes was revealed on a minute timescale.

(2) The system can reach higher system performance with the proposed control strategies under different operation stages.

(3) The impact of different heating operation strategies on system performance was quantified. The performance indicators include the collection efficiency, the storage efficiency, the solar fraction of the system and the consumption of the circulation pump on the heating side.

The frame structure of the study is presented in Figure 1. The concept of a pilot solar heating system with a solar tower receiver and STS is described in Section 2. Section 3 shows the analysis methods which include the system simulation method, operation strategies and performance evaluation metrics. Section 4 shows the validation of the system model, the assessment of the dynamic performance of the system in different operation modes, the long-term performance and the analysis of operation strategies. Finally, the main conclusions of our study are summarized in Section 5.

Preprints (www.preprints.org) | NOT PEER-REVIEWED | Posted: 17 July 2023 doi:10.20944/preprints202307.1064.v1



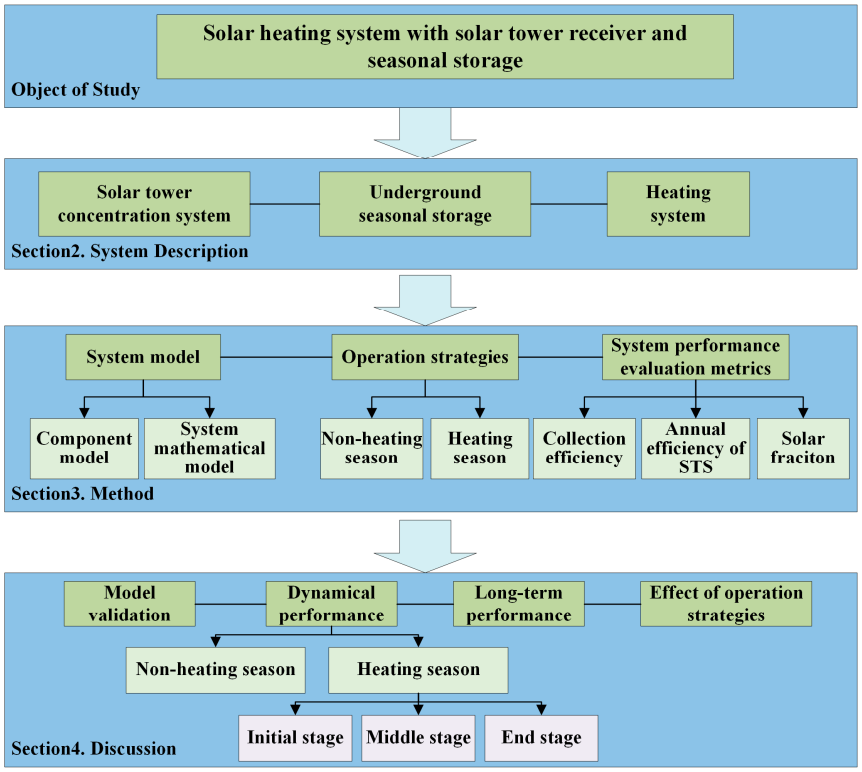


**Figure 1.** Frame structure of this paper.

## 2. System description

In this paper, a solar heating system with STS (Figure 2) is studied based on a pilot project in Huangdicheng, Hebei, China (42.23 °N, 115.43 °E). The traditional flat plate collectors in the solar heating system have relatively low efficiency at the typical supply temperatures of district heating networks (70–95°C) compared to concentrated solar thermal collectors [18]. This system adopts a concentrated solar tower receiver to utilize the solar radiation differing from the traditional solar heating system. And an underground pit thermal storage is applied to solve the problem of a mismatch between heat supply and demand in summer and winter. This water pit had 0.3 m thick concrete walls and was buried 1.0 m underground. The whole system consists of a concentrated solar thermal subsystem, an underground seasonal thermal storage unit, and a heating subsystem. A schematic of the system showing the main components is given in Figure 3. The parameters of the system are shown in Table 1.

Preprints (www.preprints.org) | NOT PEER-REVIEWED | Posted: 17 July 2023 doi:10.20944/preprints202307.1064.v1




**Figure 2.** Solar heating system with STS and solar receiver.

The complete operation cycle of the system is a year which is divided into a heat injection period (the local non-heating season) and a heat extraction period (the heating season). The operating principle of the system is that in the heat injection period, the concentrated solar thermal system charges for the STS; while during the heat extraction period, the concentrated solar thermal system (charging the buffer tank) and the STS (discharging to the buffer tank) supply heat for the building [14].

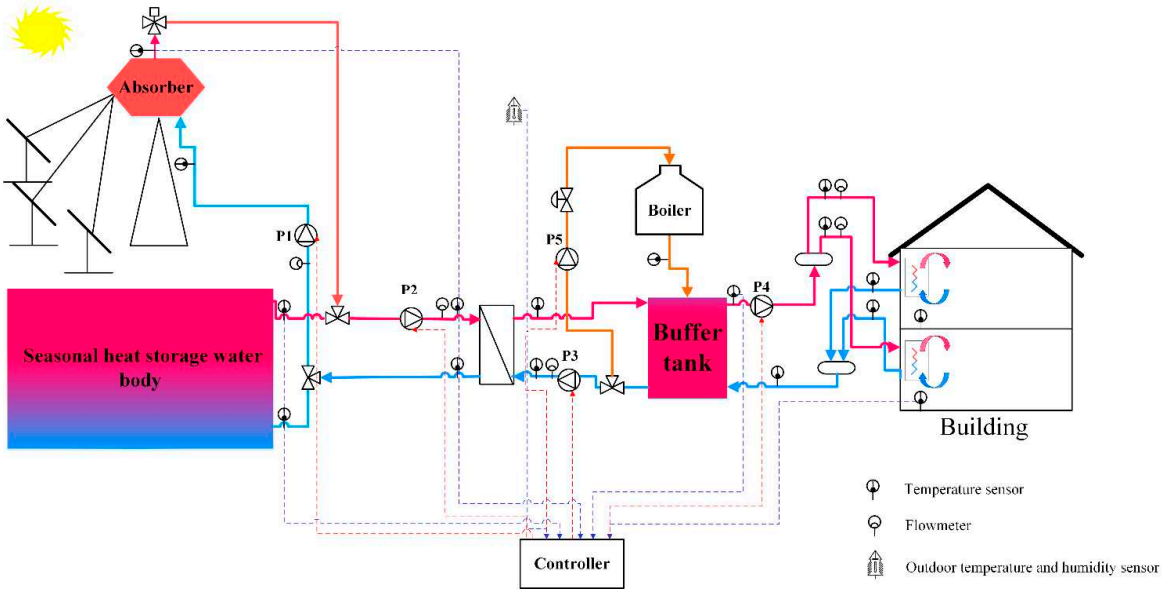


**Figure 3.** The schematic of solar heating system.

Preprints (www.preprints.org) | NOT PEER-REVIEWED | Posted: 17 July 2023 doi:10.20944/preprints202307.1064.v1



**Table 1.** System equipment parameters.

| Program | Property | Quantity | Unit |
|---|---|---|---|
| Location | Latitude | 40.23 N | ° |
| | Longitude | 115.43 E | ° |
| Heliostats field | Number of heliostats | 66 | |
| | Area of heliostat | 11.2 | $m^2$ |
| | Reflectivity | 0.9 | |
| Solar receiver | Daylighting area | 4.76 | $m^2$ |
| Buffer tank | Volume | 48 | $m^3$ |
| Seasonal thermal storage | Volume | 3000 | $m^3$ |
| Heat exchanger | Area | 30 | $m^2$ |

## 3. Methodology

To analyze the dynamic performance of the system, mathematical models of the main component and the whole system were built and the operation strategies were introduced under various operating modes.

### *3.1. System model*

The main components in this system are including STS, solar receiver, heliostat field[14], circulation pumps, buffer tank and building load. And the dynamic model of the whole system was built based on the experimental system.

#### 3.1.1. The model of STS and the solar receiver model

STS is a type of underground water pit in this system. The mathematical model is established based on the characteristics of coupled heat transfer between tank heat storage and soil. The STS model can be simplified to a one-dimensional model for the water body with a two-dimensional air layer on the top and a two-dimensional model for the soil and the concrete wall. The developed model is validated in [19].

The solar receiver is a cavity receiver installed on a 30m high tower. The model was established in MATLAB. The detailed descriptions of the model and validation were presented by [20].

#### 3.1.2. Circulation pump model

In this system, the collecting side circulation pump, the circulation pumps on both sides of the heat exchanger and the heating circulation pump are variable speed pumps. To analyze the electricity consumption of the circulation pump under different heating operating conditions, the power curves of circulation pumps were added to the model which were obtained by least square method based on the performance parameters. The performance parameters of the pump were proposed by the equipment manufacturer.

The flow-power curve of the collecting side circulation pump:

$$P_p = 0.0051F^2 + 0.052F + 0.8416 \quad (1)$$

The flow-power curve of the circulation pump on the primary side of the heat exchanger:

$$P_p = 0.00072F^2 + 0.0088F + 1.3334 \quad (2)$$

The flow-power curve of the circulation pump on the secondary side of the heat exchanger:

$$P_p = -0.0041F^2 + 0.1421F - 0.2232 \quad (3)$$

The flow-power curve of the circulation pump on the heating side:

Preprints (www.preprints.org) | NOT PEER-REVIEWED | Posted: 17 July 2023 doi:10.20944/preprints202307.1064.v1



$$P_p = -0.0000390F^2 + 0.05251F + 2.7182 \quad (4)$$

Where $P_p$ (kJ/h) is the pump power, $F$ ($m^3/h$) is the flowrate of the pump.

3.1.3. Buffer tank model

The buffer tank is assumed to be divided into multiple horizontal units. A multi-node heat transfer model was established assuming that the working medium inside the node is completely mixed.

The energy balance equation of each node in the buffer tank can be calculated with:

$$\rho_w c_{p,w} V_i \frac{dT_{w,i}}{d\tau} = Q_{in,i}(\tau) - Q_{out,i}(\tau) - Q_{loss,i}(\tau) \quad (5)$$

Where, $Q_{loss,i}(\tau)$ is the heat loss caused by heat dissipation between the surface of each node and the external environment is the heat loss caused by heat dissipation between the surface of each node and the external environment, including through the top, side walls, and bottom of the buffer tank and can be calculated with:

$$Q_{loss,i}(\tau) = U_i A_i \left(T_{w,i} - T_a\right) \quad (6)$$

Where $U_i$ (W/ ($m^2$ °C)) is the heat loss coefficient of the buffer tank, $A_i$ ($m^2$) is the area of surface of each node.

The heat and mass transfer of a node is shown in Figure 4 and the energy balance equation can be expressed as:

$$\rho_w c_{p,w} V_i \frac{dT_{w,i}}{d\tau} = \lambda_w A_w \frac{\left(T_{w,i-1} - T_{w,i}\right)}{\Delta H} + \lambda_w A_w \frac{\left(T_{w,i} - T_{w,i+1}\right)}{\Delta H} + \dot{m}_i c_{p,w}\left(T_{w,i-1} - T_{w,i}\right) + F_i^c m_h c_{p,w}\left(T_h - T_{w,i}\right) + F_i^d m_l c_{p,w}\left(T_l - T_{w,i}\right) - U_i A_i \left(T_{w,i} - T_a\right) \quad (7)$$

Where $\Delta H$ (m) is the height of the node; $T_h$ (°C) is the fluid temperature flowing into the buffer water tank at the load side; $m_h$, $m_l$ (kg/h) are the mass flow of heat source and load side flowing into the buffer tank; $F_i^d$ is the control function which determines whether the node is connected to the heat source or load side directly; $A_w$ ($m^2$) is the outer surface area of the node.

The heat loss coefficient of the buffer tank in our model was obtained through the experiment. The calculated formula can be represented as[21]:

$$U_i = \frac{Mc_{p,w}\left(T_1 - T_4\right)}{A\left(T_m - T_a\right)\Delta\tau} \quad (8)$$

Where M is the mass of water in the buffer tank (kg), $T_m$ (°C) is the average temperature of the buffer tank, $\Delta\tau$ (s) is the total time length of n tests, n is the number of tests.

Preprints (www.preprints.org) | NOT PEER-REVIEWED | Posted: 17 July 2023 doi:10.20944/preprints202307.1064.v1



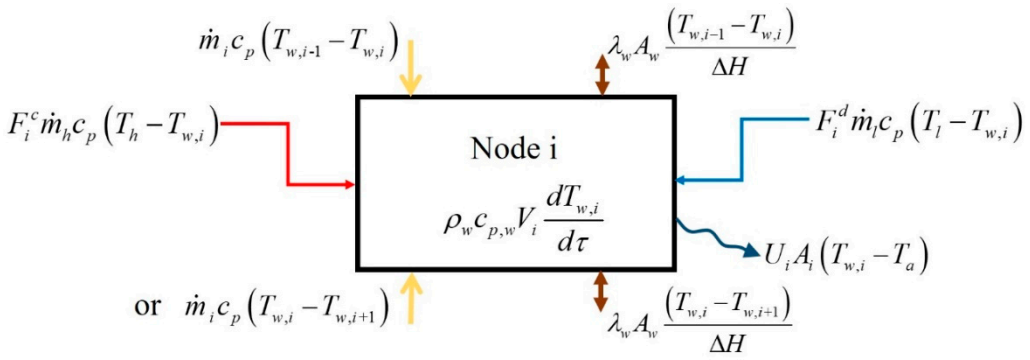


**Figure 4.** Energy transfer at a node of buffer tank.

3.1.4. Building load model

Building load is modeled using lumped parameter method. The building energy balance equation is calculated with[22]:

$$CAP\frac{dT_r}{d\tau} = \varepsilon C_{\min}\left(T_i - T_r\right) + Q_{gain} - UA\left(T_r - T_a\right) \tag{9}$$

$$Q_T = \varepsilon C_{\min}\left(T_i - T_r\right) \tag{10}$$

$$T_o = T_i - Q_T / m_h c_p \tag{11}$$

Where $\varepsilon$ is the heat exchange efficiency of the heating coil at the end of the building; $CAP$ (kJ/K) is the effective lumped heat capacity of the building; $C_{\min}$ (kJ/(h K)) is the minimum heat capacity in the heat transfer fluid on both sides of the heat exchange coil; $T_i$, $T_r$, $T_a$ (°C) are the heat source temperature in the heat exchange coil, the ambient temperature in the building and the outdoor ambient temperature, respectively; $Q_{gain}$ is the heat increment from enclosures or windows; $UA$ (kJ/(h K)) is the heat loss coefficient of the whole building; $Q_T$ is the total energy released by heat source.

3.1.5. Mathematical model of the whole system

The mathematical models of every component are listed above, and the energy transfer relationship between core components and main parameters are presented in Figure 5. As shown, the system energy transfer relationships are different under different operation modes. Thus, the mathematical equations of the whole system are established and solved falling into the following four situations.

Preprints (www.preprints.org) | NOT PEER-REVIEWED | Posted: 17 July 2023 doi:10.20944/preprints202307.1064.v1



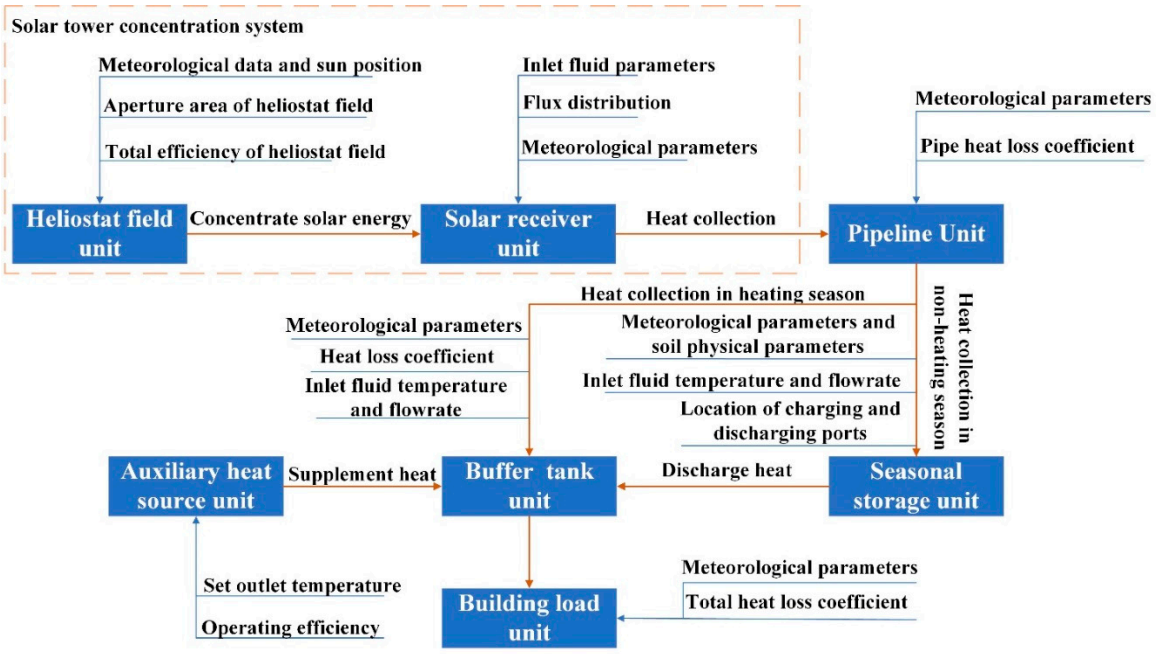


**Figure 5.** The transfer relationship of energy flow of core components.

Situation 1. In the non-heating season, the solar tower concentration system charges for the STS, the energy balance equation of the whole system can be represented as:

$$\begin{cases} \rho_{\mathrm{w}} c_{p,\mathrm{w}} V_{\mathrm{s}} \dfrac{dT_{\mathrm{w},s}}{d\tau} = Q_{\mathrm{in,s}}(\tau) - Q_{\mathrm{loss,s}}(\tau) \\ Q_{\mathrm{in,s}}(\tau) = Q_{\mathrm{rec,abs}}(\tau) = Q_{\mathrm{inc}}(\tau) - Q_{\mathrm{rec,loss}}(\tau) \\ Q_{\mathrm{inc}}(\tau) = Q_{\mathrm{solar}}(\tau) - Q_{\mathrm{h,loss}}(\tau) \\ Q_{\mathrm{inc}}(\tau) = Q_{\mathrm{solar}}(\tau) \cdot \eta_{\mathrm{h}} = N_{\mathrm{h}} \cdot A_{\mathrm{h}} \cdot I_{\mathrm{DNI}} \cdot \eta_{\mathrm{h}} \end{cases} \tag{12}$$

Where $Q_{\mathrm{h,loss}}(\tau)$ is the energy loss of the heliostat field, $Q_{\mathrm{rec,abs}}(\tau)$ is the effective heat absorption of the solar receiver, $Q_{\mathrm{loss,s}}(\tau)$ is the heat loss of STS, $Q_{\mathrm{solar}}(\tau)$ is the solar energy absorbed by the solar tower concentration system, $Q_{\mathrm{inc}}(\tau)$ is the solar energy incident on the system.

Situation 2. In the non-heating season, the solar tower concentration system charges for the buffer tank when the maximum temperature of the STS exceeds 90 °C. The energy balance equation of the whole system can be expressed as:

$$\begin{cases} \rho_{\mathrm{w}} c_{p,\mathrm{w}} V_b \dfrac{dT_{\mathrm{w,b}}}{d\tau} = Q_{\mathrm{in,b}}(\tau) - Q_{\mathrm{loss,b}}(\tau) - Q_{\mathrm{supply,b}}(\tau) \\ Q_{\mathrm{in,b}}(\tau) = Q_{\mathrm{rec,abs}}(\tau) = Q_{\mathrm{inc}}(\tau) - Q_{\mathrm{rec,loss}}(\tau) \\ Q_{\mathrm{inc}}(\tau) = Q_{\mathrm{solar}}(\tau) - Q_{\mathrm{h,loss}}(\tau) \end{cases} \tag{13}$$

Where $Q_{\mathrm{in,b}}(\tau)$ is the heat inputted to the buffer tank, $Q_{loss,b}(\tau)$ is the heat loss of the buffer tank, $Q_{\mathrm{supply,b}}(\tau)$ is the heat supplied by buffer tank.

Situation 3. In the heating season, the solar tower concentration system charges for the buffer tank. The buffer water tank supplies heat to the building directly when the heat of the buffer tank can meet the heat load demand. The energy balance equation of the whole system can be shown as:

Preprints (www.preprints.org) | NOT PEER-REVIEWED | Posted: 17 July 2023 doi:10.20944/preprints202307.1064.v1



$$\begin{cases} CAP\dfrac{dT_{\mathrm{r}}}{d\tau}=Q_{\mathrm{in,r}}(\tau)+Q_{\mathrm{gain,r}}(\tau)-Q_{\mathrm{loss,r}}(\tau) \\ Q_{\mathrm{in,r}}(\tau)=Q_{\mathrm{supply,b}}(\tau)=Q_{\mathrm{in,b}}(\tau)-Q_{\mathrm{loss,b}}(\tau)-\rho_{\mathrm{w}}c_{p,\mathrm{w}}V_{b}\dfrac{dT_{\mathrm{w},b}}{d\tau} \\ Q_{\mathrm{in,b}}(\tau)=Q_{\mathrm{rec,abs}}(\tau)=Q_{\mathrm{inc}}(\tau)-Q_{\mathrm{rec,loss}}(\tau) \\ Q_{\mathrm{inc}}(\tau)=Q_{\mathrm{solar}}(\tau)-Q_{\mathrm{h,loss}}(\tau) \end{cases} \tag{14}$$

Where $Q_{\mathrm{in,r}}(\tau)$ is the heat input to the building; $Q_{\mathrm{loss,r}}(\tau)$ is the heat loss of the building.

Situation 4. In the heating season, the solar tower concentration system and the STS charge for the buffer tank. The buffer water tank provides heat for the building. When the heat of the buffer tank cannot meet the heat load demand, the auxiliary heat source supplies heat to buildings. The unsteady mathematical model of the system can be expressed as:

$$\begin{cases} CAP\dfrac{dT_{\mathrm{r}}}{d\tau}=Q_{\mathrm{in,r}}(\tau)+Q_{\mathrm{gain,r}}(\tau)-Q_{\mathrm{loss,r}}(\tau) \\ Q_{\mathrm{in,r}}(\tau)=Q_{\mathrm{supply,b}}(\tau)=Q_{\mathrm{in,b}}(\tau)-Q_{\mathrm{loss,b}}(\tau)-\rho_{\mathrm{w}}c_{p,\mathrm{w}}V_{\mathrm{b}}\dfrac{dT_{\mathrm{w,b}}}{d\tau} \\ Q_{\mathrm{in,b}}(\tau)=Q_{\mathrm{rec,abs}}(\tau)+Q_{\mathrm{discharge,s}}(\tau)+Q_{\mathrm{aux}}(\tau) \\ Q_{\mathrm{rec,abs}}(\tau)=Q_{\mathrm{solar}}(\tau)-Q_{\mathrm{h,loss}}(\tau)-Q_{\mathrm{rec,loss}}(\tau) \\ Q_{\mathrm{discharge,s}}(\tau)=\rho_{\mathrm{w}}c_{p,\mathrm{w}}V_{\mathrm{s}}\dfrac{dT_{\mathrm{w,s}}}{d\tau}-Q_{\mathrm{loss,s}}(\tau) \end{cases} \tag{15}$$

Where $Q_{\mathrm{aux}}(\tau)$ is the heat supplemented by an auxiliary heat source.

Each module is connected through energy flow and combined with the system operation strategy. A solar heating system with a solar tower receiver and STS was finally built in TRNSYS 17.02 coupled with MATLAB. The dynamic operation characteristics and operation strategy of the system can be studied and analyzed on the platform. The system model is shown in Figure 6 and the descriptions of each module are shown in Table 2. The time step of the system model is 60s[19]. The tolerance convergence of the system model is 0.001. And the working fluid in this system is pure water assuming incompressible.

Preprints (www.preprints.org) | NOT PEER-REVIEWED | Posted: 17 July 2023 doi:10.20944/preprints202307.1064.v1



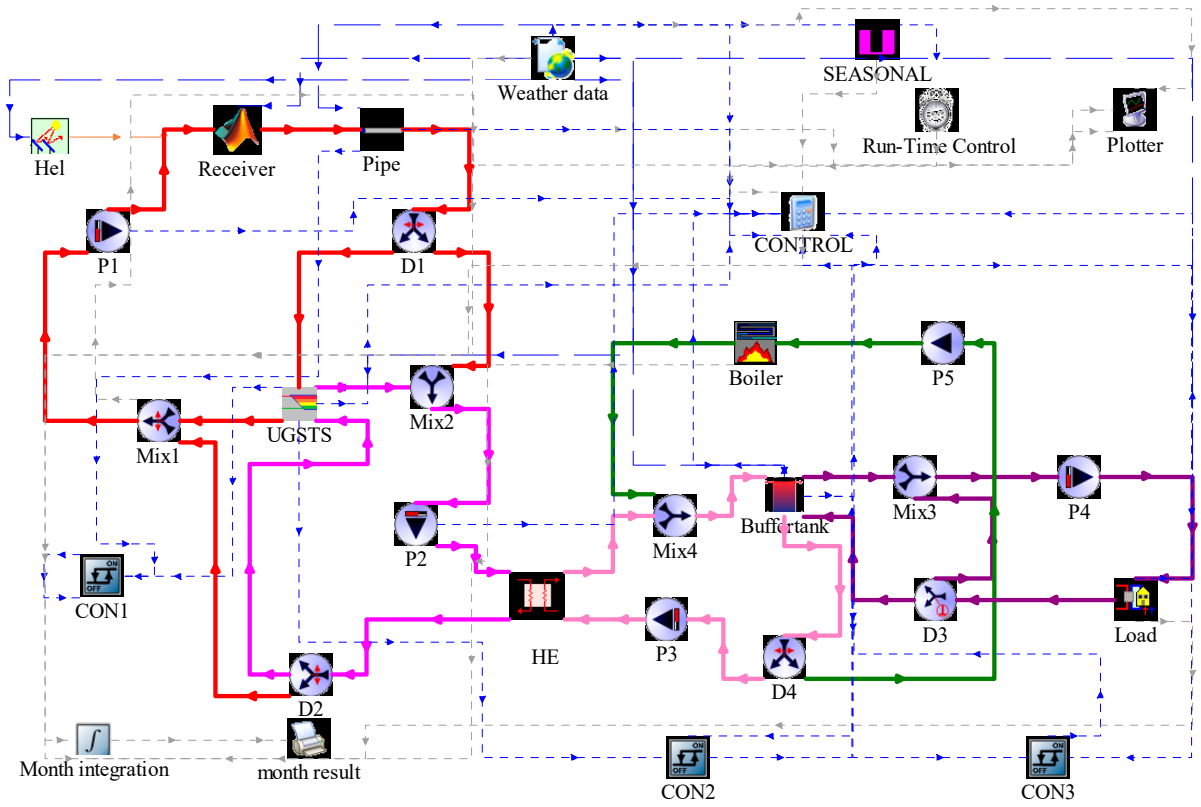


**Figure 6.** TRNSYS simulation platform for the solar heating system.

**Table 2.** Main modules and parameters of the TRNSYS simulation platform.

| Project | Name | Type | Notes |
|---|---|---|---|
| Meteorological parameters | Weather data | Type 15-3 | Calling in Typical annual meteorological data of Huailai obtained from the EnergyPlus website |
| Heliostat field | Hel | Type 394 | Calling in instantaneous efficiency of the heliostat field |
| Receiver | Receiver | Type 155 | Calling in structural parameters and mathematical models in MATLAB |
| Circulating pump | P(1~5) | Type 110 | Input the power curve of each circulation pump |
| Underground seasonal thermal storage | UGSTS | Type 207 | Self-developed model |
| Buffer tank | Buffer tank | Type 531 | Measured heat loss coefficient 0.34 W/(m²·°C) |
| Operation control unit | CON (1~3) | Type 2b | Temperature difference control |
| | CONTROL | Calculator | Logical control |
| Data display or output | Plotter | Type 65d | Display of results |
| | Month result | Type 25c | Output of results |
| Diversion valve | D (1~4) | Type 11f | Switch between different circulation routes |
| Mixing valve | M (1~4) | Type 11d | Switch between different circulation routes |

| | | | |
|---|---|---|---|
| Heat exchanger | HE | Type 5b | Counterflow, average heat transfer coefficient 100 W/K per m² of collector area [23] |
| Building load | LOAD | Type 12c | Heat load per unit heating area 40 W/m² |
| Heating season controller | SEASONAL | Type 14 | The heating season is from November 1st to April 1st of the following year |
| Auxiliary fuel boiler | Boiler | Type 700 | Rated power 170 kW, Boiler efficiency 0.9 |
| Temperature control diverter valve | D5 | Type 11b | The water supply temperature can reach the set temperature by mixing the supply and return water |

*3.2. Operation strategies*

According to the performance of main components and different operation modes, the control strategies are divided into the following situations.

3.2.1. Operation strategy in the non-heating season

In the constant temperature operation control strategy, the system performance is more prominent than the temperature difference control in the non-heating season as mentioned in [14]. Thus, the constant temperature operation control strategy is adopted in this paper. The outlet temperature of the solar tower concentration system is set to be 10 ℃ higher than the temperature of the top layer of the STS to prevent damage to the temperature stratification of the STS. By adjusting the flowrate of the circulation pump, the outlet temperature of the solar tower concentration system can reach the set value.

3.2.2. Operation strategy in the heating season

The solar tower concentration system still worked with the constant temperature operation control strategy. The outlet temperature of the solar tower concentration system is set to be 10 ℃ higher than the temperature of the top layer of the buffer tank.

The operation and regulation of the solar heating system with STS is more complicated than the conventional heating system in the heating season. On the one hand, the temperature of the STS keeps decreasing in the heating season and there is no heat pump in the system. On the other hand, the heat load decreased with the increase of outdoor temperature at the beginning and end of the heating season, while the temperature of the STS is relatively high at the beginning of the heating season. Thus, there is an obvious mismatch between the heat supply temperature and the demand temperature. This will lead to many problems, including the waste of useful energy in STS, significant heat loss in pipelines, destruction of temperature stratification in STS and a decrease in the efficiency of the solar collection system. Therefore, it is necessary to propose a reasonable heating operation strategy. The control strategy of the heating circulation pump adopted the combination of quality-quantity regulation and staged variable flow quality regulation in this study[24].

When the solar tower concentration system isn't operating or the heat collection of the solar tower concentration system doesn't meet the heat demand. The STS will operate in discharging mode. The discharge flowrate of the STS adopted the quantity regulation principle which is the district heating regulation method[24]. Thus, the circulation pumps on both sides of the heat exchanger adopted the quantity regulation.

The circulation pump of the auxiliary heat source will start when the STS and solar tower concentration system can't meet the heat demand. And constant flow control was used.

*3.3. System performance evaluation metrics*

1. Solar energy absorbed by the solar tower concentration system can be calculated with:

Preprints (www.preprints.org) | NOT PEER-REVIEWED | Posted: 17 July 2023 doi:10.20944/preprints202307.1064.v1



$$Q_{\text{solar}} = \int_{\tau 1}^{\tau 2} N_{\text{h}} \cdot A_{\text{h}} \cdot I_{\text{DNI}} d\tau \tag{16}$$

Where $N_{\text{h}}$ is the number of heliostats on the daylighting surface of the solar receiver at the current time, $A_{\text{h}}$ ($m^2$) is the aperture area of a single heliostat, $I_{\text{DNI}}$ ($W/m^2$) is the direct normal irradiance.

2. Effective heat gain of the solar tower concentration system can be calculated with:

$$Q_{col} = \int_{\tau 1}^{\tau 2} c_p \cdot m \cdot \left(T_{rec,out} - T_{rec,in}\right) d\tau \tag{17}$$

Where $Q_{col}$ (J) is the heat effectively collected by the solar receiver, $c_p$ is the heat capacity of water, m (kg/s) is the mass flow of water, $T_{rec,in}$ (°C) is the inlet temperature of the solar receiver, $T_{rec,out}$ (°C) is the outlet temperature of solar receiver.

3. Collection efficiency of the solar tower concentration system can be calculated with:

$$\eta_{\text{col}} = \frac{Q_{col}}{Q_{solar}} \tag{18}$$

4. The Annual efficiency of STS can be expressed as:

$$\eta_{\text{n}} = 1 - \frac{Q_{loss}}{Q_{charge}} \tag{19}$$

$$Q_{charge} = \int_0^{\tau} c_p \cdot m \cdot \left(T_{in,s} - T_{out,s}\right) d\tau \tag{20}$$

$$Q_{discharge} = \int_0^{\tau} c_p \cdot m \cdot \left(T_{out,s} - T_{in,s}\right) d\tau \tag{21}$$

$$Q_{loss} = Q_{charge} - Q_{discharge} - Q_{st} \tag{22}$$

Where $Q_{charge}$ is the heat charged into the STS, $Q_{\text{discharge}}$ is the heat discharged from STS, $Q_{\text{loss}}$ is the heat loss of STS, $Q_{st}$ is the energy change in seasonal thermal energy storage, $T_{in,s}$ is the temperature of water inflow during heat charging, $T_{out,s}$ is the temperature of outflow water during heat charging.

5. Solar fraction can be expressed as [25]:

$$SF = \frac{Q_{sol}}{Q_{load}} \tag{23}$$

where $Q_{sol}$ is the heat supplied by solar energy for heating in the system, $Q_{load}$ is the total heat load of the system.

## 4. Discussion

### *4.1. Model validation*

The models of underground seasonal storage and solar receiver have been validated by [19] [20]. The measured data from October 1, 2018 to October 7, 2018 were selected to verify the system simulation model. Since the solar tower concentration system charges for the STS in actual operation, the inlet and outlet temperature of the solar receiver and the internal temperature distribution of the STS are used for comparison between the experiment and simulation. The root-mean-square deviation (RMSD), the average relative error (ARE), and the maximum relative error (MRE) are listed in Table 3.

$$RMSD = \sqrt{\frac{\sum_{j=1}^{N} (T_{j,\text{exp}} - T_{j,sim})}{N}} \tag{24}$$

$$ARE = \frac{1}{N} \sum_{j=1}^{N} \frac{(T_{j,\text{exp}} - T_{j,sim})}{T_{j,\text{exp}}} \times 100\% \tag{25}$$

Preprints (www.preprints.org) | NOT PEER-REVIEWED | Posted: 17 July 2023 doi:10.20944/preprints202307.1064.v1



$$MRE = MAX\left(\frac{\left|T_{j,\exp} - T_{j,sim}\right|}{T_{j,\exp}}\right)\times 100\% \tag{26}$$

In this study, the measured parameters are the temperatures and flowrates. The uncertainty of the above parameters is calculated as follows[26]:

$$\delta R = \sqrt{\sum_i^N \left(\frac{\partial R}{\partial X_i}\delta X_i\right)^2} \tag{27}$$

Where, $R$ and $\delta R$ are measured parameter and the uncertainty. $X_i$ and $\delta X_i$ are measurement value and the accuracy of test equipment. The accuracy of test equipment and the uncertainties in experimental results are shown in Tables 4 and 5.

The comparisons of the experimental results and simulation of the inlet and outlet temperature of the solar receiver are shown in Figure 7. The results showed that the measured values of the outlet temperature of the solar receiver were in good agreement with the simulated values for a continuous week. The simulation results were slightly different from the experimental values, only when the circulation pump started and stopped. The reason was that the heat transfer caused by the oscillating flow in the receiver tubes was not considered in the simulation model when the circulation pump starts and stops. However, the maximum deviation of inlet and outlet temperature of solar receiver was not greater than 3 ℃ and the average error of outlet temperature is 2.57%. Thus, the overall simulation model can reflect the dynamic operation performance of the solar receiver under different weather conditions.

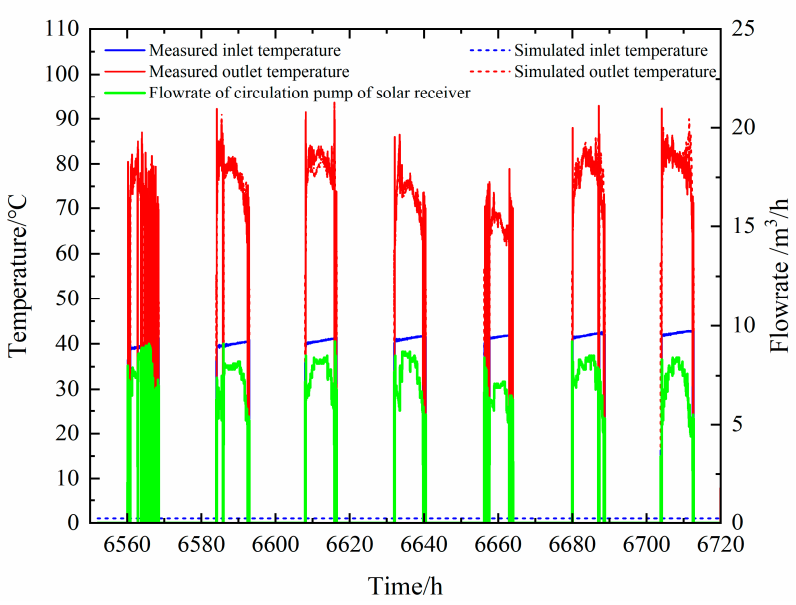


**Figure 7.** Simulated and measured inlet and outlet of solar tower concentration system.

The comparations of experimental results and simulation values of the temperature at different heights in the STS are shown in Figure 8. The simulation results agreed well with the experimental values. There were some deviations between the simulated values and the experimental values at the top two measurement points. The reason was that soil moisture was affected by environmental temperature and humidity, which had a certain impact on the heat transfer between water and soil. However, this was not considered in this model. The maximum deviation between the experimental value and the simulated value of temperature in each layer was not greater than 1.0 ℃ and the maximum error is 1.85%.

Preprints (www.preprints.org) | NOT PEER-REVIEWED | Posted: 17 July 2023 doi:10.20944/preprints202307.1064.v1



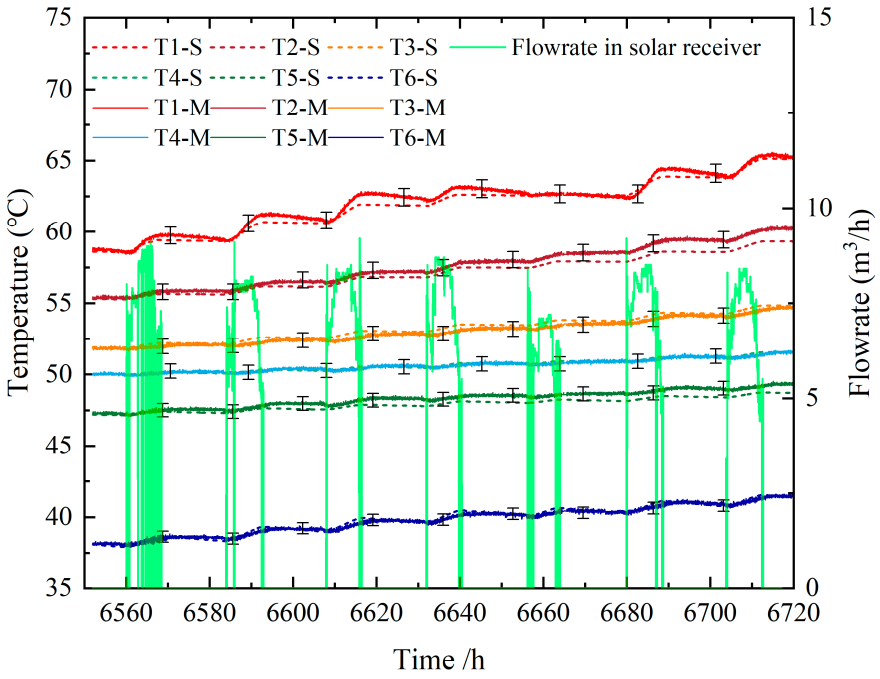


**Figure 8.** Experimental and simulation values of temperature at different heights in STS (S-simulation, M-measured).

**Table 3.** RMSE and maximum relative errors of the numerical results.

| Location | RMSD (℃) | ARE (%) | MRE (%) |
|---|---|---|---|
| T1 (4.25m from STS bottom) | 1.10 | 0.42 | 1.52 |
| T2 (3.45m from STS bottom) | 1.54 | 0.75 | 1.85 |
| T3 (2.65m from STS bottom) | 0.79 | 0.45 | 0.28 |
| T4 (1.85m from STS bottom) | 0.32 | 0.03 | 0.57 |
| T5 (1.05m from STS bottom) | 1.23 | 0.75 | 1.63 |
| T6 (0.25m from STS bottom) | 0.50 | 0.12 | 0.92 |
| Inlet temperature of receiver | 1.12 | 2.49 | 6.0 |
| Outlet temperature of receiver | 3.01 | 2.57 | 9.8 |

**Table 4.** Test equipment and specifications

| Measurement devices | Type | Range | Accuracy |
|---|---|---|---|
| Temperature sensor | PT100 | 0～100 ℃ | ±0.5 ℃ |
| Vortex Flowmeter | HH-HYBLWGY-50 | 0～25 m³/h | ±1.0% |

**Table 5.** Test equipment and specifications

| Parameters | Type of data | Unit | Relative error |
|---|---|---|---|
| Average inlet temperature of solar receiver | Measured | ℃ | 3.783% |
| Average outlet temperature of solar receiver | Measured | ℃ | 2.049% |
| Average flowrate | Measured | m³/h | 1.058% |
| Average temperature of STS | Measured | ℃ | 0.983% |

The results indicated that the simulated values of the system were in good agreement with the experiment values. Therefore, the system model can accurately reflect the dynamic operation characteristics and the performance of the system.

Preprints (www.preprints.org) | NOT PEER-REVIEWED | Posted: 17 July 2023 doi:10.20944/preprints202307.1064.v1



*4.2. Dynamical performance of the system*

Due to the instability of solar radiation and the heat demand of buildings, solar heating system work under variable working conditions. In this section, the dynamical performance was analyzed with a dynamic simulated method in a typical day or typical operation modes, and the switch mechanism between multiple operation modes was also revealed.

The local typical yearly meteorological data and the heat demand of the 3000 m² building which was calculated by the system model were shown in Figure 9. The annual heat load of the system was 1571976.2 MJ. Solar radiation was relatively low from October to March of the next year. This is also the local heating season. The total horizontal solar radiation and the ambient temperature reached the minimum around January, while the building heat load reached the maximum. And the total horizontal solar irradiation is relatively high in the rest of the year, during which there is no heat demand. Therefore, there is a serious mismatch between solar resources and demand. And that means a waste of solar energy in summer and a lower solar fraction, which is the typical problem of the solar heating system in northern China. Thus, the solar heating system with STS in this paper can effectively solve the above problems. Moreover, the system has the advantages of reducing heating costs and achieving stable continuous operation with high efficiency.

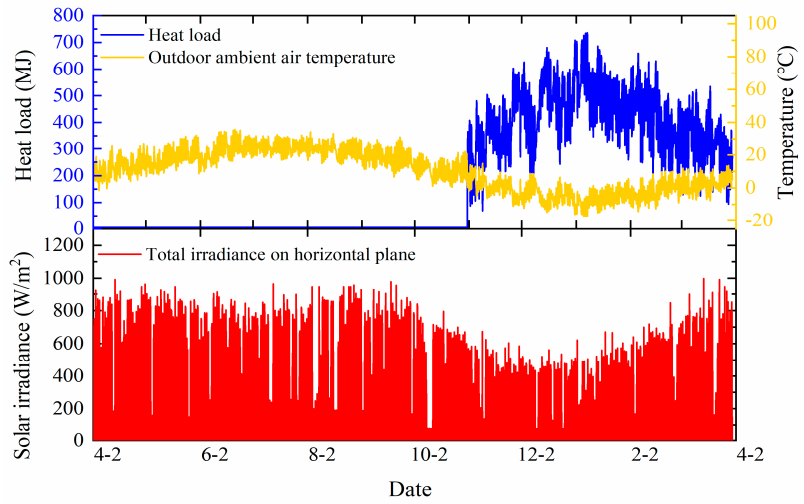


**Figure 9.** Local typical annual meteorological data and heating load

4.2.1. Dynamic characteristics analysis of typical working conditions in the non-heating season

In the non-heating season, the working fluid is pumped from the bottom of the STS to the solar tower concentration system, and then heated by the solar receiver and charged to the top of STS. The dynamic operation characteristics of the solar tower receiver in a typical day and the temperature change process of STS over a continuous week were analyzed with minute-level measured meteorological data. The inlet temperature of the solar receiver and the top temperature of the STS were set to 60 °C and 80 °C, respectively. In constant temperature mode, the outlet temperature of the solar receiver was set to 10 °C higher than the top temperature of the STS. The dynamic performance of the solar receiver on a typical day was shown in Figure 10. The typical day is cloudy and the maximum DNI of the whole day was 550 W/m². Severe fluctuations of solar radiation occurred around 3:30 p.m. owing to the influence of clouds. Therefore, the flowrate of the circulation pump of solar receiver fluctuated greatly when the solar radiation changed violently. When the solar irradiance fluctuates, it is necessary to continuously adjust the flowrate of the solar receiver circulation pump to ensure that the outlet temperature of the solar receiver reaches the set temperature. As shown in Figure 10, the changing trend of flowrate was consistent with that of DNI. The outlet temperature of the solar receiver remained around 90 °C throughout the day, which was 10 °C higher than the temperature of the STS.

Preprints (www.preprints.org) | NOT PEER-REVIEWED | Posted: 17 July 2023 doi:10.20944/preprints202307.1064.v1



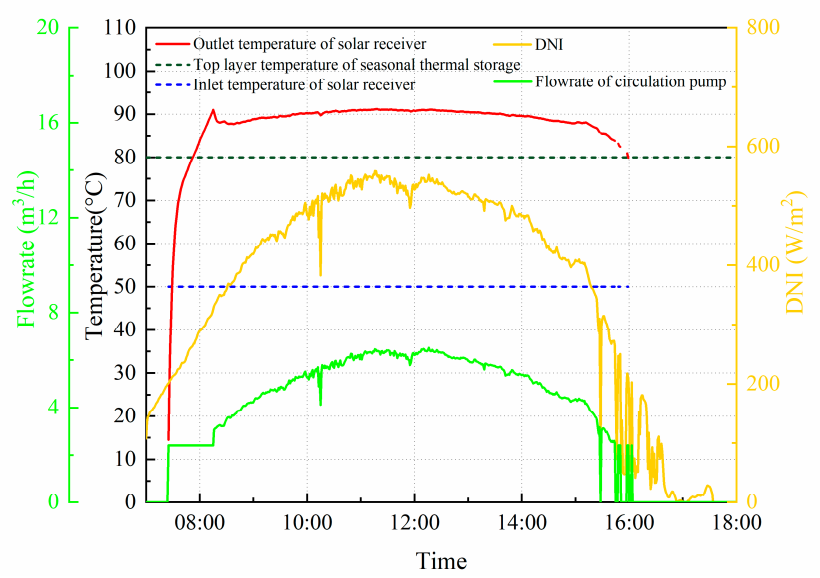


**Figure 10.** Dynamic operation performance of solar receiver on a typical day.

As shown in Figure 11, the solar tower concentration system ran continuously for one week in constant temperature mode and the dynamic performances of the solar receiver and STS were presented. The measured temperature stratification of STS was imported as the initial condition. Regardless of various solar irradiation conditions such as cloudy or sunny, the solar receiver can maintain a good operating state during the continuous operation of a week. The outlet temperature of the solar receiver was ensured to be 10 ℃ higher than the top temperature of the STS by dynamically adjusting the circulation pump flowrate under different solar irradiation conditions. The temperature stratification in the STS was maintained well and the temperature of each layer kept rising. Due to the proximity of the charging port to the top layer and the high charging temperature, the top layer temperature rose more obviously than the bottom layer. As a consequence, the temperature stratification in the STS had been effectively improved. Temperature stratification is one of the important criteria for evaluating the performance of sensible heat storage. And it determines the efficiency of STS and the entire solar heating system. Good temperature stratification not only improves the available heat of the system, but also plays an important role in improving the heat collection efficiency of the solar tower concentration system and reducing the heat loss of STS.

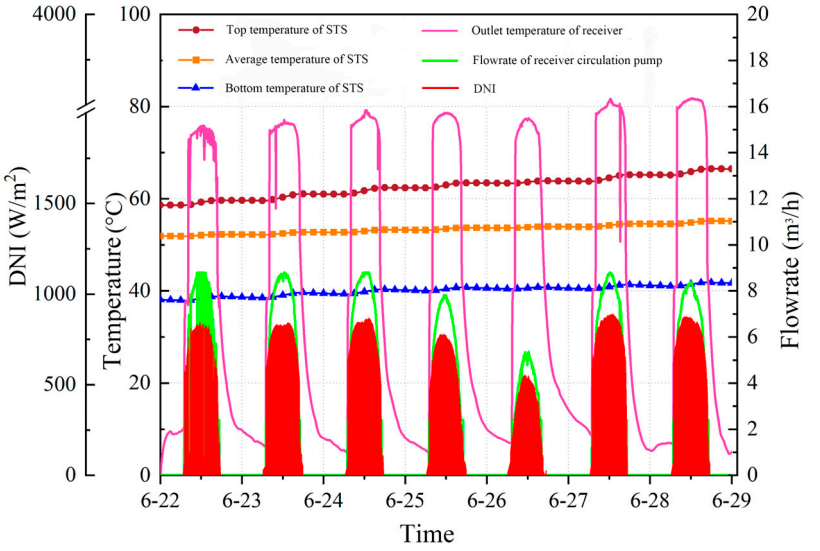


**Figure 11.** Performance of continuous operation for one week.

Preprints (www.preprints.org) | NOT PEER-REVIEWED | Posted: 17 July 2023 doi:10.20944/preprints202307.1064.v1



4.2.2. Dynamic characteristics analysis of typical working conditions in the heating season

The operation performance of the solar heating system must be evaluated on the premise of satisfying the continuous and stable energy supply and ensuring the thermal comfort of users. The solar fraction and heating stability of the solar heating system are effectively improved by STS. The operation state of the system in the heating season is more complex than that in the non-heating season. The STS which is a supplementary heat source has a higher temperature in the initial stage of the heating season, while the required heating temperature is lower. The supply and required heating temperature temperatures don't match and the temperature of the STS gradually decreases. For the above operating characteristics, the heating season is divided into the initial stage, the middle stage and the end of the heating season. The dynamic operation characteristics of the STS under different operating conditions and the switching mechanism of multiple modes are analyzed.

**1.** In the initial stage of the heating season

The outdoor ambient temperature and the temperature in the STS are both high, while the building load and the required heating temperature are both low during this period. The solar tower concentration system can basically meet the building load. The STS supplies heat to buildings through heat exchangers when the solar radiation is poor or no solar radiation. The minute level measured meteorological data of two consecutive days (November 27-28, 2018) was selected to analyze the dynamic operation performance of the system. The initial temperature of the buffer water tank is set to 35 ℃ and the top temperature of the STS water is set to 80 ℃. Based on the heating control strategy proposed in this study, the heating supply temperature of the system is adjusted with the change of ambient temperature. The supply temperature increases when the outdoor ambient temperature decreases.

As shown in Figure 12, as the outdoor ambient temperature decreased, the building heat load increased accordingly. There were three times of discharge of the STS during the two consecutive days. The solar tower concentration system stopped running after 5 p.m. The buffer tank was used for heating preferentially. When the temperature of the upper layer of the buffer tank dropped to 5 ℃ higher than the supply temperature, the STS started to charge for the buffer tank until the upper layer temperature rose to 15 ℃ higher than the supply temperature, in order to ensure the stability of system heating and reduce the starting and stopping times of the circulation pump of the STS. Furthermore, when the outdoor environment temperature increase, the discharge power of STS will decrease to achieve efficient and reasonable utilization of stored heat. The system can continuously and stably supply heat under the dynamic changes of solar radiation resources and building load. The indoor temperature of the building was maintained at around 20 ℃, which basically met the thermal comfort of users.

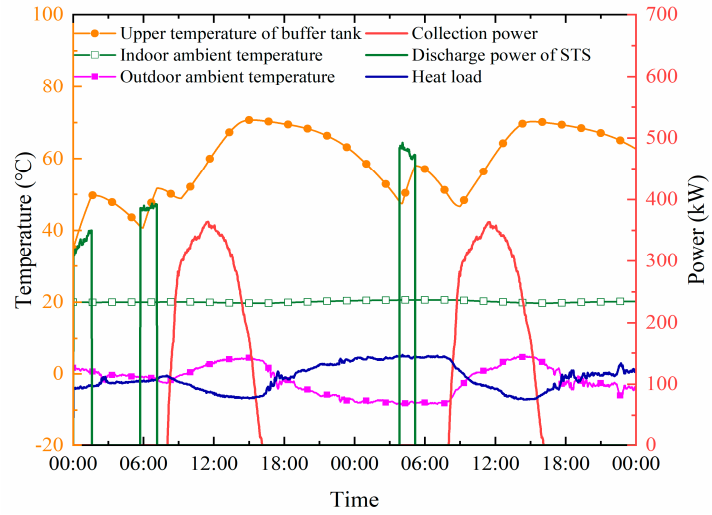


**Figure 12.** Dynamic operation performance at the beginning of heating season.

Preprints (www.preprints.org) | NOT PEER-REVIEWED | Posted: 17 July 2023 doi:10.20944/preprints202307.1064.v1



**2.** In the middle stage of the heating season

The middle stage of the heating season refers to the time when the outdoor ambient temperature basically reaches the lowest and the heat load reaches the highest throughout the year. And the temperature of the STS continuously decreases to the required water supply temperature. The solar tower concentration system heats the building directly, basically meeting the heat demand when the solar radiation is good. Minutely measured meteorological data on January 20th, 2018 were selected to analyze the dynamic operation of system heating. The initial temperature of the buffer tank was set at 45 °C.

The heating control strategy of the system in the middle stage of the heating season is the same as that in the initial stage. As shown in Figure 13, when the temperature of the top layer of the STS dropped to only 1 °C higher than the supply temperature, the auxiliary boiler was used to supplement the heat until the temperature of the upper layer of the buffer tank was higher than the supply temperature or the solar tower concentration system started. In the middle of the heating season, it is mainly affected by the dynamic changes of solar radiation resources, building load and discharging temperature of STS. There were three operation modes: direct heating of the solar tower concentration system, discharging of STS and auxiliary boiler heating. The system can supply heat continuously and stably, and the indoor temperature of the building was kept at about 20 °C.

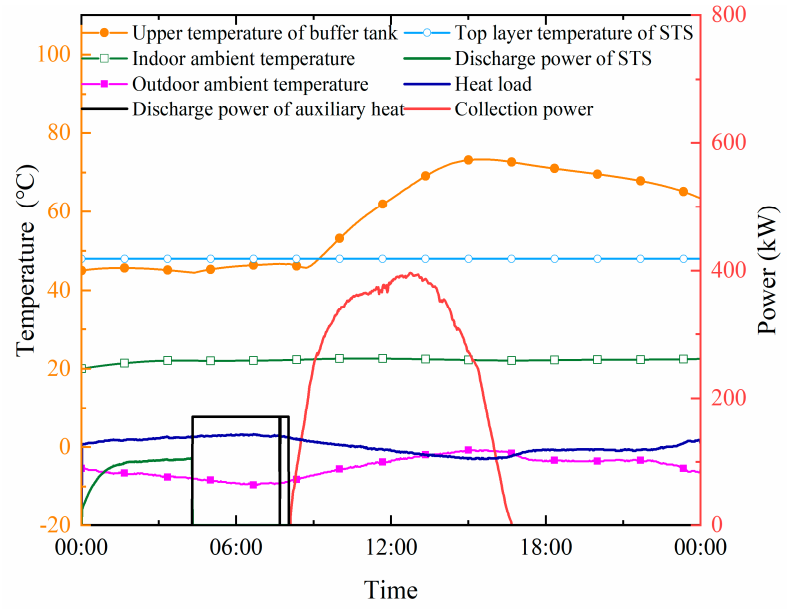


**Figure 13.** Dynamic operation performance in the mid-heating season.

**3.** In the end of heating season

In the end of the heating season, the outdoor ambient temperature gradually increases, and the heat load and supply temperature gradually decrease. At the same time, the temperature of the STS may still be higher than the supply temperature, although it continues to decline. Minute-level measured meteorological data for two consecutive days (March 1-2, 2019) were selected to analyze the dynamic performance of the system. The initial temperature of the buffer tank was set at 45 °C.

The system heating regulation strategy at the end of the heating season is the same as the above stages. The solar tower concentration system provided heat to the buffer tank when the solar radiation was sufficient. When the solar tower concentration system stopped running, the heat stored in the buffer tank was used preferentially for heating after 5:00 p.m. on March 1st. It was cloudy on March 2nd, and the direct heating of the solar tower concentration system basically met the heat demand. When the temperature of the upper layer of the buffer tank dropped to 5 °C higher than the supply temperature, the STS was used for heat supplement such as around 2:00 a.m. on March 1st shown in Figure 14. Between 3:00 a.m. and 8:00 a.m., the auxiliary boiler ran until the start of the solar

Preprints (www.preprints.org) | NOT PEER-REVIEWED | Posted: 17 July 2023 doi:10.20944/preprints202307.1064.v1



tower concentration system. There were three operation modes to switch: direct heating of the solar tower concentration system, discharging of STS and auxiliary boiler heating.

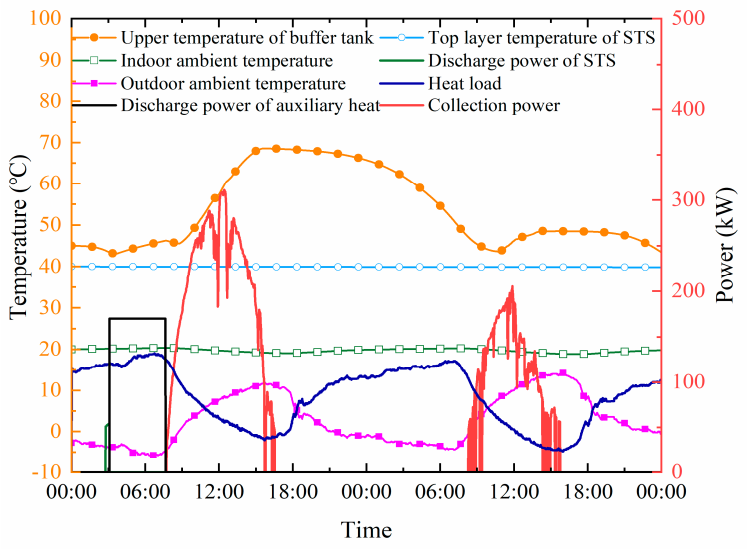


**Figure 14.** Dynamic operation performance at the end of the heating season.

*4.3. Long-term performance of the system*

To analyze the dynamic performance in different time dimensions, the operating characteristics of the system for one year and three consecutive years were simulated with the local typical meteorological data. The initial temperature of STS and the surrounding soil was set to 14 ℃ and 8 ℃ according to the measured data. The simulation results of the outlet temperature of the solar receiver and the temperature change of the STS in the first year were shown in Figure 15.

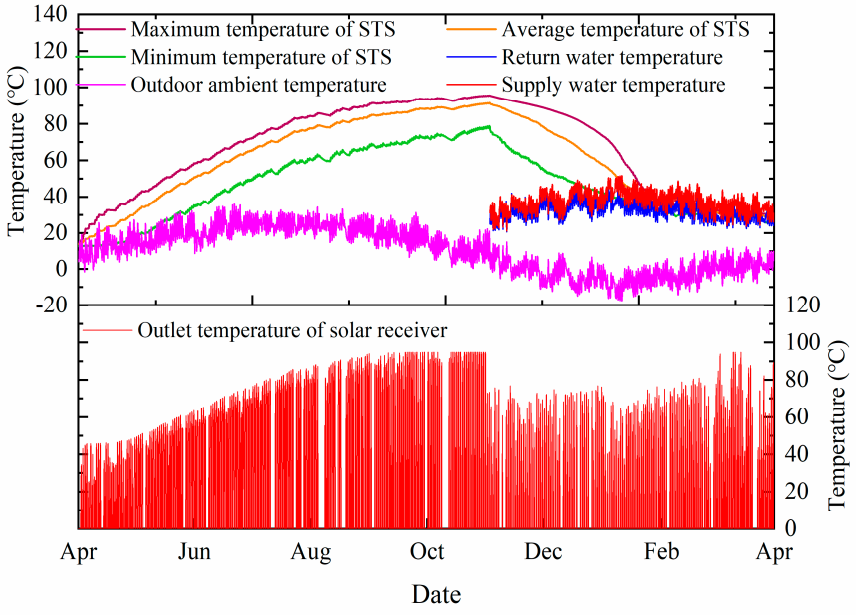


**Figure 15.** Annual operation performance of the system.

In the non-heating season, the average temperature of STS increased from 14.0 ℃ to 84.7 ℃ and dropped to 35.9 ℃ until the end of the heating season. To avoid damaging the temperature stratification in the STS, the outlet temperature of the solar receiver was set to be higher than the water temperature at the top of the STS, approaching 90 ℃ at the end of the non-heating season

Preprints (www.preprints.org) | NOT PEER-REVIEWED | Posted: 17 July 2023 doi:10.20944/preprints202307.1064.v1



(August to October). In the heating season, the operating temperature of the solar receiver was affected by the buffer tank. The outlet temperature of the solar receiver was set to be higher than the supply temperature and the buffer tank basically met the heat demand, at the end of the heating season. As a result, the solar receiver also operated at a higher temperature. As the traditional flat plate collectors in solar heating system have relatively low efficiency at the typical supply temperatures of district heating networks (70–95°C) compared to the concentrated solar thermal collectors. Thus, the solar tower concentration system in this paper has certain advantages at the end of the non-heating season and the heating season.

The energy flow of the solar heating system in the first year was shown in Figure 16. The solar tower concentration system collected 591.6 MWh heat in the whole year and the annual average thermal efficiency is 50.2%. In the non-heating season, with the gradual increase of the storage capacity and average temperature of the STS, the heat loss also increased. In September and October, due to the lower DNI and the higher operating temperature of the solar receiver and the STS, the heat collection increased less and the heat loss of the STS increased; In the heating season, the solar tower concentration system supplied heat to users through charging the buffer tank. At the beginning of the heating season (November and December), the heat supplied by the heat collection system and STS can meet the heat demand, and the solar fraction can reach 100%. In the middle of the heating season (January), the auxiliary heat source will supplement 25.3 MWh in January. At the end of the heating season (February and March), the heating temperature required by the user side is relatively low. The supplementary heat of the auxiliary heat source is less with 9.7 MWh. Most of the heat came from the solar tower concentration system. The annual solar fraction of the system can reach 85.9% with 375.1 MWh. And the annual efficiency of the STS is 56.1%. Furthermore, the heat stored in the STS can be effectively extracted throughout the heating season.

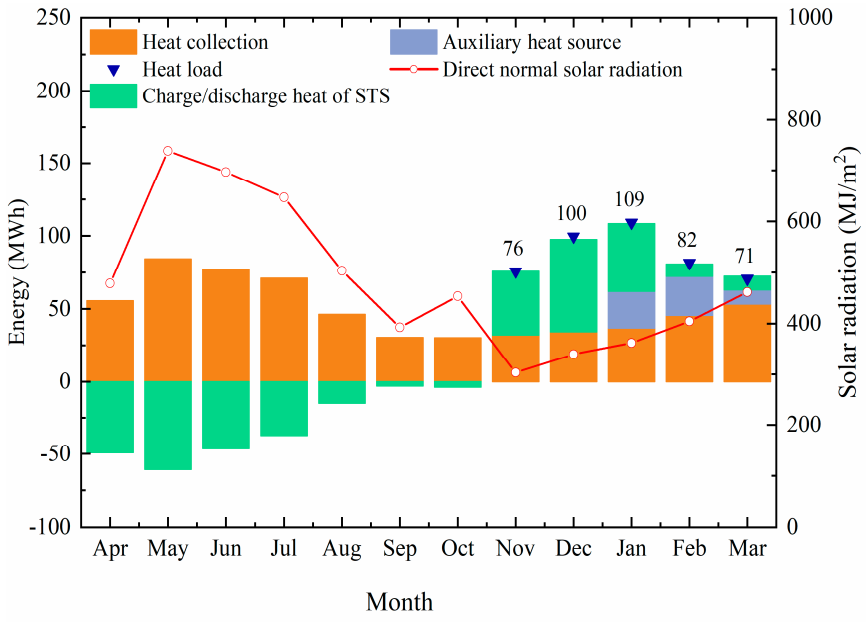


**Figure 16.** Operation energy flow in the first year.

The temperature change of the STS for three consecutive years was shown in Figure 17. It showed that the average temperature of STS at the end of the heating season was 35.9 °C in the first year. In the second year, the initial temperature of the STS and the operating temperature of the system were higher at the end of the non-heating season. The annual average efficiency of the solar tower concentration system and the heat charging to the STS in the second and third years gradually decreased.

Preprints (www.preprints.org) | NOT PEER-REVIEWED | Posted: 17 July 2023 doi:10.20944/preprints202307.1064.v1



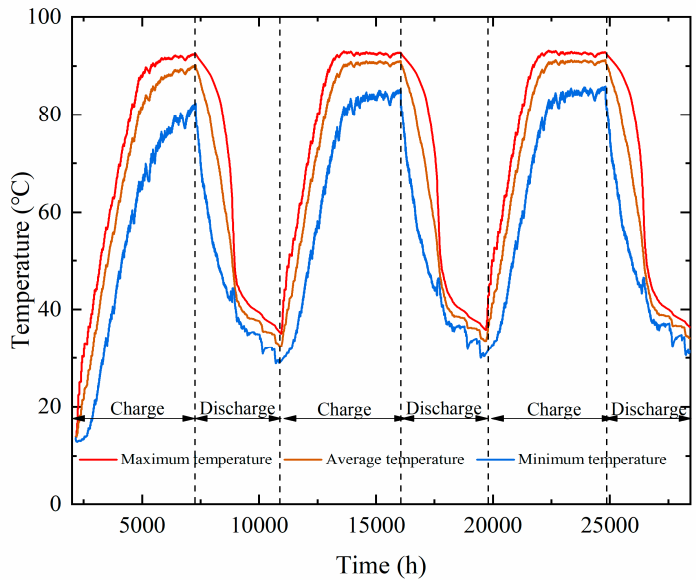


**Figure 17.** Temperature changes of STS for three consecutive years.

As shown in Figure 18, the heat discharged from the STS increased year by year. In the third year, the discharged heat reached 186.1 MWh and the annual storage efficiency was 57.5%. The temperature of the soil gradually improved and reached an equilibrium state. It was remarkable that a heat pump was not added to this system and the heat in the STS was not completely used up in the first year. This led to a higher initial temperature in the second year. Furthermore, the solar fraction of the system was gradually improved. The solar fraction of the system reached 89.4% in the third year, which was 3.6% higher than the first year.

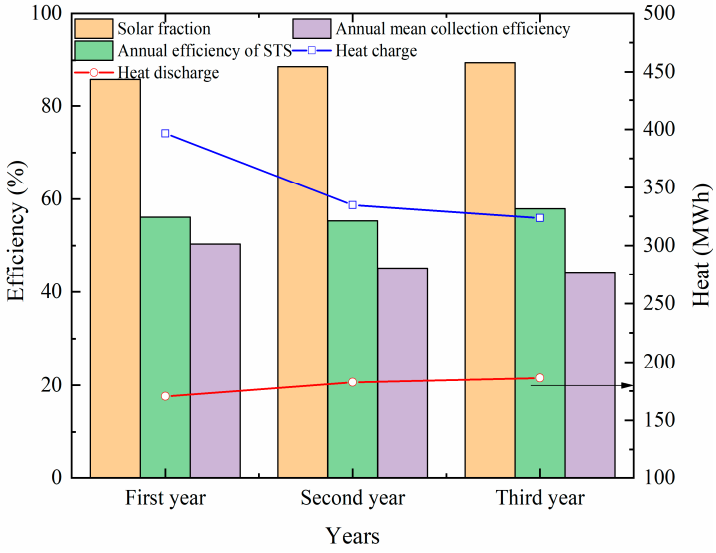


**Figure 18.** System performance change over three continuous years.

*4.4. Effect of operation strategies*

In this section, the impact of different heating operation strategies on system performance was analyzed. This included quantity regulation, quality regulation, constant temperature and flowrate regulation and the quantity-quality regulation which was proposed in this paper. The influence of the heating strategy was assessed by the performance indicators such as the collection efficiency, the storage efficiency, the solar fraction of the system and the consumption of the circulation pump on the heating side. The heat discharged by the STS needs to be effectively utilized to realize the stable heating of the system during the heating season. However, the temperature of the STS gradually

Preprints (www.preprints.org) | NOT PEER-REVIEWED | Posted: 17 July 2023 doi:10.20944/preprints202307.1064.v1



decreased during the operation. If the quantity regulation and constant temperature and flow heating control modes were adopted, the heating temperature was always set to constant temperature operation (such as 55 °C). In addition, if the heat pump or reheating method is not used, the heat stored in the STS can't be effectively used and the STS is in a static heat dissipation state when the temperature of the STS drops below 55 °C. As a result, the solar fraction and the annual efficiency of STS will be lower and the electricity consumption of the circulation pump with quantity regulation was lower than that with constant temperature and flow regulation (Figure 19). The quality regulation and quantity-quality regulation improved the solar fraction and the annual average efficiency of the solar tower concentration system compared with the other two methods. On the one hand, the heat stored in the STS can be fully utilized. On the other hand, the heat loss of the pipe network could be reduced. The electricity consumption of the pump was 18.4 MWh in the quality control. However, when the quantity-quality regulation method was adopted, it can be significantly reduced to 10.2 MWh, a reduction of 44.6%. The solar fraction of the system was also 17.5% higher than that of constant temperature and flowrate control.

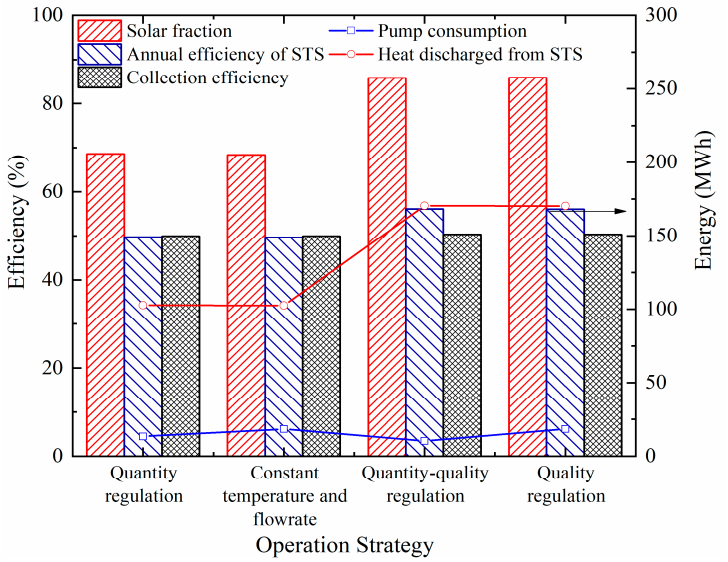


**Figure 19.** System performance under different heating strategies.

As shown in Figure 20, in the quantity-quality regulation strategy, the STS discharged heat every month during the heating season. The solar fraction of the system can reach 100% in November and December. The heat discharged from the STS accounted for 13% of the total heat supply in March of the next year. However, under the constant temperature and flowrate mode, the solar fraction of the system reached 100% only in November and the STS discharged heat only in November and December, accounting for 58% of the heat supply in that month.

Preprints (www.preprints.org) | NOT PEER-REVIEWED | Posted: 17 July 2023 doi:10.20944/preprints202307.1064.v1



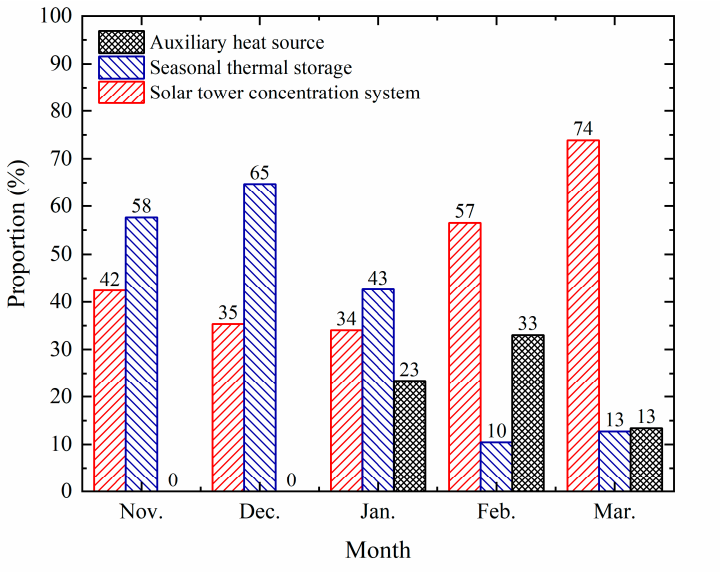


(**a**) Quantity-quality regulation

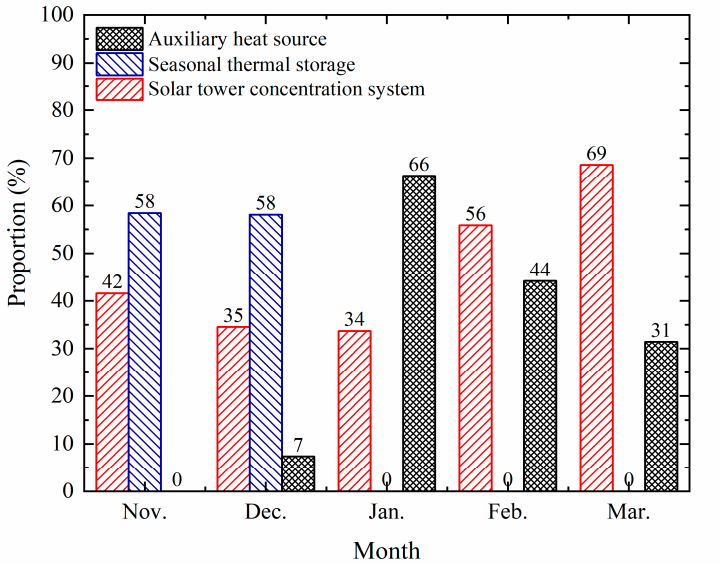


(**b**) Constant temperature and flowrate

**Figure 20.** The Contribution rate of different heat sources.

## 5. Conclusion

A pilot solar heating system with a solar tower receiver and STS was established. The dynamic performances of the system in different time scales were studied. Furthermore, a comparative study was conducted to investigate the influence of the operation strategies. The main conclusions are as follows:

(1) The solar heating system with STS in our study has outstanding performance in different time scales. And through the switching of multiple operation modes, the system can operate stably and continuously under the fluctuation of solar radiation resources and heat demand. The significant mismatch between solar energy and heat load in northern China can be resolved.

(2) The quality-quantity operation strategies can be effective ways to improve the discharge efficiency of the STS and the system performance without the heat pump to utilize the thermal stored in the STS when the temperature of the STS is below the traditional heating supply temperature. The annual solar fraction of the system could be reached 85.9%. And the annual efficiency of STS was 56.1%. The electricity consumption of the pump on the heating side could be significantly reduced by 44.6% compared with the quality control.

(3) The solar fraction of the system was gradually improved. The solar fraction of the system reaches 89.4% in the third year, which is 3.6% higher than the first year. Although the solar tower collection system can improve the collection efficiency at the higher temperature, the operational temperature still affects the system performance, especially in the third year. Thus, reasonable control strategies of the whole system should be analyzed in different time dimensions, such as the long-term period.

(4) In order to promote the development of solar heating system with STS, scientific design methods for system configuration and operation strategies need to be addressed in the future. Based on the perfect forecasts for the weather and the SDH loads, the development of optimized control strategies is the focus of future research.

**Acknowledgments:** The work has been supported by Key R&D Plan Projects in Gansu Province (22YF7GA162) and the National Key R&D Program of China (2021YFE0113500). And thanks for the Foundation of Key Laboratory of Solar Power System Engineering (2023SPKL02).

## Nomenclature

| | |
|---|---|
| ***Latin characters*** | |
| $A$ | Area, $m^2$ |
| $C$ | Heat capacity, kJ/(h·k) |
| $CAP$ | Effective lumped heat capacity of building, kJ/K |
| $c_p$ | Specific heat capacity, J/kg·K |
| $F_i^d$ | Control function |
| $F$ | Flowrate, $m^3$/h |
| H | Heigh, m |
| $I_{\mathrm{DNI}}$ | Normal direct irradiance, W/$m^2$ |
| m | Mass flowrate, kg/h |
| M | Mass, kg |
| N | Number |
| $P$ | Power, kJ/h |
| Q | Heat, J |
| T | Temperature, °C |
| $U_i$ | Heat loss coefficient, W/ ($m^2$ °C) |
| $UA$ | Heat loss coefficient of the building, kJ/(h·K) |
| V | Volume, $m^3$ |
| ***Abbreviations*** | |
| STS | Seasonal thermal storage |
| SGHP | Solar and ground source heat pump system |
| DNI | Direct normal irradiance |
| SGSP | Salt gradient solar pond |
| UGSTS | Underground seasonal thermal storage |
| SF | Solar fraction |
| RMSD | Root-mean-square deviation |
| ARE | Average relative error |
| MRE | Maximum relative error |
| ***Subscripts*** | |
| a | Ambient |
| abs | Effective heat absorption |
| aux | Auxiliary heat source |
| b | Buffer tank |
| col | Heat collected by solar receiver |
| charge | Charge into the STS |
| discharge | Heat discharged from STS |
| exp | Experiment |
| h | Heat source/heliostat field |
| i | Natural numbers from 1 to n |
| in | Inflow |

| | |
|---|---|
| inc | Incident energy on the solar receiver |
| gain | Increment |
| l, load | Load side |
| max | Maximum |
| min | Minimum |
| out | Outflow |
| p | Pump |
| r | Room |
| rec | Receiver |
| *Solar* | Solar tower concentration system |
| S, s | Seasonal storage |
| *sim* | Simulation |
| w | Water |
| ***Greek character*** | |
| $\varepsilon$ | Heat exchange efficiency |
| $\rho$ | Density, kg/m³ |
| $\tau$ | Time, s |
| $\lambda$ | Thermal conductivity, W/m/°C |

## References


1. Center, B.E.C.R. Annual Development Research Report on Building Energy Efficiency in China 2022 2022, 1–23.
2. Rghif, Y.; Zeghmati, B.; Bahraoui, F. Numerical Analysis of the Influence of Buoyancy Ratio and Dufour Parameter on Thermosolutal Convection in a Square Salt Gradient Solar Pond. *Fluid Dyn. Mater. Process.* **2022**, *18*, 1319–1329, doi:10.32604/fdmp.2022.021500.
3. Rghif, Y.; Zeghmati, B.; Bahraoui, F. Modeling the Influences of a Phase Change Material and the Dufour Effect on Thermal Performance of a Salt Gradient Solar Pond. *Int. J. Therm. Sci.* **2021**, *166*, 106979, doi:10.1016/j.ijthermalsci.2021.106979.
4. Rghif, Y.; Bahraoui, F.; Zeghmati, B. Experimental and Numerical Investigations of Heat and Mass Transfer in a Salt Gradient Solar Pond under a Solar Simulator. *Sol. Energy* **2022**, *236*, 841–859, doi:10.1016/j.solener.2022.03.033.
5. Rghif, Y.; Colarossi, D.; Principi, P. Effects of Double-Diffusive Convection on Calculation Time and Accuracy Results of a Salt Gradient Solar Pond: Numerical Investigation and Experimental Validation. *Sustainability* **2023**, *15*, 1479, doi:10.3390/su15021479.
6. Tosatto, A.; Dahash, A.; Ochs, F. Simulation-Based Performance Evaluation of Large-Scale Thermal Energy Storage Coupled with Heat Pump in District Heating Systems. *J. Energy Storage* **2023**, *61*, 106721, doi:10.1016/j.est.2023.106721.
7. Narula, K.; Oliveira, F. De; Villasmil, W.; Patel, M.K. Simulation Method for Assessing Hourly Energy Fl Ows in District Heating System with Seasonal Thermal Energy Storage. *Renew. Energy* **2020**, *151*, 1250–1268, doi:10.1016/j.renene.2019.11.121.
8. Ushamah, H.M.; Ahmed, N.; Elfeky, K.E.; Mahmood, M.; Qaisrani, M.A.; Waqas, A.; Zhang, Q. Techno-Economic Analysis of a Hybrid District Heating with Borehole Thermal Storage for Various Solar Collectors and Climate Zones in Pakistan. *Renew. Energy* **2022**, *199*, 1639–1656, doi:10.1016/j.renene.2022.09.059.
9. Kim, M.H.; Kim, D.; Heo, J.; Lee, D.W. Techno-Economic Analysis of Hybrid Renewable Energy System with Solar District Heating for Net Zero Energy Community. *Energy* **2019**, *187*, 115916, doi:10.1016/j.energy.2019.115916.
10. Chu, S.; Sethuvenkatraman, S.; Goldsworthy, M.; Yuan, G. Techno-Economic Assessment of Solar Assisted Precinct Level Heating Systems with Seasonal Heat Storage for Australian Cities. *Renew. Energy* **2022**, *201*, 841–853, doi:10.1016/j.renene.2022.11.011.
11. Renaldi, R.; Friedrich, D. Techno-Economic Analysis of a Solar District Heating System with Seasonal Thermal Storage in the UK. *Appl. Energy* **2019**, *236*, 388–400, doi:10.1016/j.apenergy.2018.11.030.
12. Zhang, C.; Nielsen, E.; Fan, J.; Furbo, S. Thermal Behavior of a Combi-Storage in a Solar-Ground Source Heat Pump System for a Single-Family House. *Energy Build.* **2022**, *259*, doi:10.1016/j.enbuild.2022.111902.
13. Maragna, C.; Rey, C.; Perreaux, M. A Novel and Versatile Solar Borehole Thermal Energy Storage Assisted by a Heat Pump. Part 1: System Description. *Renew. Energy* **2023**, *208*, 709–725, doi:10.1016/j.renene.2023.03.105.
14. Li, X.; Wang, Z.; Li, J.; Yang, M.; Yuan, G.; Bai, Y. Comparison of Control Strategies for a Solar Heating System with Underground Pit Seasonal Storage in the Non-Heating Season. *J. Energy Storage* **2019**, *26*, 100963, doi:10.1016/j.est.2019.100963.

15. Villasmil, W.; Troxler, M.; Hendry, R.; Schuetz, P.; Worlitschek, J. Control Strategies of Solar Heating Systems Coupled with Seasonal Thermal Energy Storage in Self-Sufficient Buildings. *J. Energy Storage* **2021**, *42*, doi:10.1016/j.est.2021.103069.
16. Wang, Y.; Rao, Z.; Liu, J.; Liao, S. An Optimized Control Strategy for Integrated Solar and Air-Source Heat Pump Water Heating System with Cascade Storage Tanks. *Energy Build.* **2020**, *210*, 109766, doi:10.1016/j.enbuild.2020.109766.
17. Zhao, J.; Lyu, L.; Li, X. Numerical Analysis of the Operation Regulation in a Solar Heating System with Seasonal Water Pool Thermal Storage. *Renew. Energy* **2020**, *150*, 1118–1126, doi:10.1016/j.renene.2019.10.077.
18. Tian, Z.; Perers, B.; Furbo, S.; Fan, J. Annual Measured and Simulated Thermal Performance Analysis of a Hybrid Solar District Heating Plant with Flat Plate Collectors and Parabolic Trough Collectors in Series. *Appl. Energy* **2017**, *205*, 417–427, doi:10.1016/j.apenergy.2017.07.139.
19. Bai, Y.; Wang, Z.; Fan, J.; Yang, M.; Li, X.; Chen, L.; Yuan, G.; Yang, J. Numerical and Experimental Study of an Underground Water Pit for Seasonal Heat Storage. *Renew. Energy* **2020**, *150*, 487–508, doi:10.1016/j.renene.2019.12.080.
20. Li, X.; Wang, Z.; Li, J.; Chen, L.; Bai, Y.; Yang, M.; Guo, M.; Sun, F.; Yuan, G. Numerical and Experimental Study of a Concentrated Solar Thermal Receiver for a Solar Heating System with Seasonal Storage. *Int. J. Energy Res.* **2021**, 1–17, doi:10.1002/er.6341.
21. GB/T18708-2002. Test Methods for Thermal Performance of Domestic Solar Water Heating System.
22. Reference, M. TRNSYS 17 Manual. *Math. Ref.* 4.
23. Pahud, D. CENTRAL SOLAR HEATING PLANTS WITH SEASONAL DUCT STORAGE AND SHORT-TERM WATER STORAGE : DESIGN GUIDELINES OBTAINED BY DYNAMIC SYSTEM SIMULATIONS. **2000**, *69*, 495–509.
24. Xiaoxia, L.; Zhifeng, W.; Jinping, L.; Yang, M.; Bai, Y.; Chen, L. *Space Heating Management for Solar Heating System with Underground Pit Storage*; 2020; Vol. III; ISBN 9789811395277.
25. Ciampi, G.; Rosato, A.; Sibilio, S. Thermo-Economic Sensitivity Analysis by Dynamic Simulations of a Small Italian Solar District Heating System with a Seasonal Borehole Thermal Energy Storage. *Energy* **2018**, *143*, 757–771, doi:10.1016/j.energy.2017.11.029.
26. Moffat, R.J. Describing the Uncertainties in Experimental Results. *Exp. Therm. Fluid Sci.* **1988**, *1*, 3–17, doi:10.1016/0894-1777(88)90043-X.